Cancer Cell International

RESEARCH

Open Access

Enhancing antitumor immunity in Lewis lung cancer through plasma-treated medium-induced activation of dendritic cells

Chae Bok Lee[1†], Hei Gwon Choi[2,6], Sintayehu Kebede Gurmessa[3], In-Taek Jang[1], Naresh Kumar[4], Zongyou Jiang[1], Nagendra Kumar Kaushik[5] and Hwa-Jung Kim[1*]

Abstract

Background Recently, atmospheric non-thermal plasma jet-treated medium (PTM) has been recognized as a novel strategy in cancer therapy and lymphocyte activation. However, PTM has limitations in inducing a robust antitumor-immune response. This study demonstrated that PTM treatment inhibited tumor progression by activating dendritic cells (DCs).

Method In this study, we investigated the effects of PTM on selective cytotoxicity and intracellular reactive oxygen species (ROS) generation and oxidative stress-mediated signaling (e.g., glutathione peroxidase, catalase) using respective fluorescence probes in Lewis lung cancer (LLC) cells. Then, the PTM affects the expression of interferon-gamma (IFN)-γ-induced programmed death-ligand 1 (PD-L1) and inhibition of signal transducer and activator of transcription 1 (STAT1) in LLC cells using immunoblotting. Additionally, PTM effects on the tumor cell's death and activation of DCs were done by co-culturing DCs with or without tumor cells. Further, a mouse model was used to evaluate the synergistic antitumor effects of PTM and DCs where tumors are grown under the skin.

Results PTM-exposed tumor cells increase intracellular superoxide production, enhancing ROS generation and leading to cancer immunogenic cell death. In addition, PTM suppresses IFN-γ-induced PD-L1 expression and STAT1 activation in tumor cells. The activation of DCs induced by PTM is downregulated when these cells are co-cultured with tumor cells. In vivo, intraperitoneal injection of PTM-activated DCs, as a synergistic agent to intertumoral PTM treatment, led to increased $CD4^+$ and $CD8^+$ T cell infiltration into the tumor and spleen and eventually decreased tumor growth.

Conclusion Overall, this research introduces a promising avenue for improving lung cancer treatment using PTM to stimulate an immune response and induce cell death in tumor cells. Further studies will be essential to validate these findings and explore clinical applications.

Keywords Non-thermal plasma-treated medium, Reactive oxygen species, Dendritic cell activation, Lewis Lung cancer cells, Cancer immunogenic cell death, Programmed death-ligand 1

†Chae Bok Lee is first author.

*Correspondence:
Hwa-Jung Kim
hjukim@cnu.ac.kr

Full list of author information is available at the end of the article

Graphical Abstract

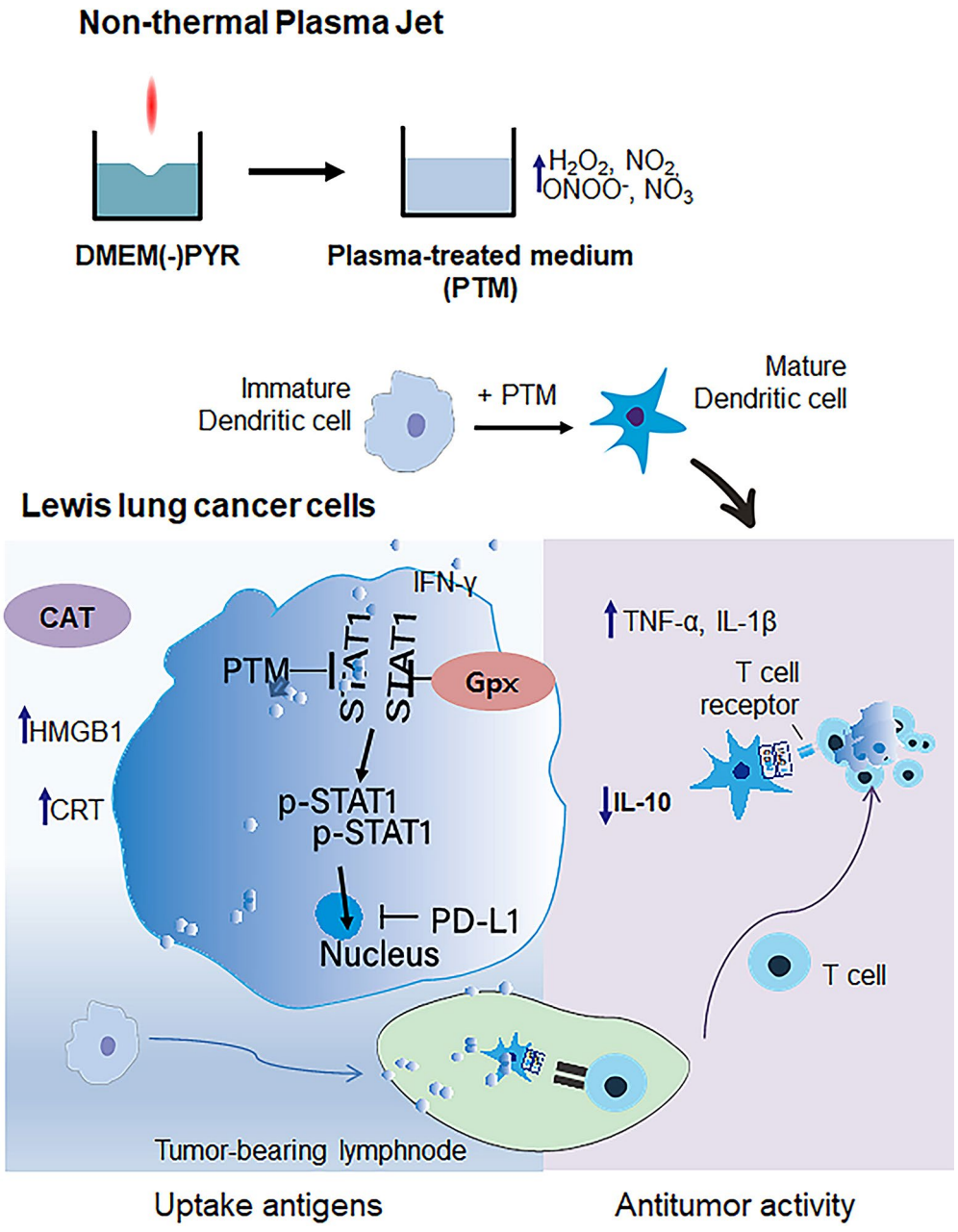

Background

Despite advancements in immunotherapy, non-small cell lung cancer (NSCLC) remains challenging to treat due to its heterogeneity and suppressive effects of the tumor microenvironments on T-cell activation [1–3]. However, dendritic cells (DCs) are central to the immune response, acting as antigen-presenting cells and contributing to tumor progression [4–6]. Their dual role complicates their use in immunotherapy [7]. The maturation of DCs is crucial for effective T-cell activation, which is essential for successful immunotherapy. Insufficient T-cell activation in lung cancer immunotherapy was addressed using hydrogen peroxide (H2O2)-treated dendritic cells, which showed heightened efficacy in increasing T-cell proliferation [8], where DCs play a crucial role. This highlights the need for novel strategies to overcome these challenges.

On the other hand, plasma-treated medium (PTM) containing a mix of reactive oxygen species (ROS) and reactive nitrogen species (RNS), such as hydrogen peroxide (H_2O_2), nitrite (NO_2^-), nitrate (NO_3^-),

and peroxynitrite ($ONOO^-$) represents an innovative approach [8–11]. PTM aims to induce oxidative and nitrosative stress in cancer cells [8, 12], potentially leading to their death while stimulating the immune system [13, 14]. It was shown that PTM-induced immunogenic cell death (ICD) stimulates the adaptive immune system [10, 15], but further research is crucial to understand the reactive species in NSCLC fully and to develop more effective immunotherapies.

In the present study, we chose the Lewis lung cancer (LLC) cell line because of its high aggressiveness [16] and the complexity of lung tissue. Exposure to PTM increases intracellular superoxide levels and ROS generation, contributing to immunogenic cell death (ICD) in LLC cells. We also investigated the selective toxicity between normal lung MRC-5 cells and LLC cells. PTM demonstrates selective toxicity towards cancer cells over normal lung cells, crucial for minimizing collateral damage [12, 17]. Further, stress-related genes such as glutathione peroxidase (Gpx1) and catalase (CAT) expression were studied, which helped understand PTM effects' mechanisms. Moreover, PTM-induced immunogenic cell death (ICD), including markers like calreticulin (CRT) and high mobility group box 1 (HMGB1), was analyzed using Immunofluorescence, which is beneficial for triggering an adaptive immune response [18–20].

Additionally, PTM's impact on PD-L1 and STAT1 was analyzed, which suggests potentially modulating immune checkpoints to enhance the immune response against tumors [21]. Furthermore, Flow cytometry results showed that PTM affects DC surface markers (CD80, MHCII, CD40), indicating enhanced DC activation and potential for improved antigen presentation [22]. We also explored a novel approach to improving antitumor activity in the subcutaneous mice model by combining PTM-stimulated DCs into the intraperitoneal and intratumor. PTM treatment shows promise in enhancing antitumor activity. The present study demonstrates that a plasma-treated medium (PTM) enhances the production of reactive oxygen species (ROS), leading to oxidative stress-mediated immunogenic cell death, which could be an alternative therapeutic strategy for treating NSCLC. The findings suggest that PTM could be a viable alternative or adjunct to existing therapies for NSCLC. By enhancing ROS production and inducing ICD, PTM may overcome some of the limitations of traditional immunotherapies and provide a novel strategy for treating NSCLC.

Methods

Plasma-treated medium

The experimental setup of the atmospheric pressure plasma jet (APPJ) was used [23]. This device consisted of a nitrogen (N_2) gas cylinder, a gas flow regulator, a power controller, and a manmade plasma source head, and it was similar to a previously described system [24]. Nitrogen (99.99%) flow rate was set to 1.5 L/min. PTM was prepared by exposing 0.5 mL of Dulbecco's modified Eagle medium (DMEM) (Sigma, D5796) without sodium pyruvate (PYR) in a 24-well culture plate (SPL, 37024) to plasma for 5 min. The distance between the APPJ and the medium surface was 5 mm. PTM was diluted in a cell culture medium and used immediately or in advanced preparation at −80 ℃ or 4 ℃.

H2O2 and NO2 analyses

To measure H_2O_2 generation in PTM, we used the colorimetric method using a working solution comprising 100 µL of 10U/mL horseradish peroxidase (A22188, Invitrogen, Carlsbad, CA, USA) stock solution and 50 µL of 10 mM concentration Amplex™ Red. Additionally, NO_2 was analyzed using the Griess reagent assay, which comprises 1% naphthyl ethylene dihydrochloride and 0.1% sulfanilamide (Sigma Aldrich), as a standard, which was diluted in a deionized water using a nitrite (100 mM).

Antibodies and reagents

Rabbit anti-phospho-signal transducer and activator of transcription 1 (p-STAT1) (1:1000), STAT1 (1:1000), and β-Actin antibodies (1:1000) were purchased from Cell Signaling Technology. Mouse Recombinant interferon-γ (IFN-γ, 094-04701) was purchased from Wako. PD-L1 was purchased from Anticam (1:1000, ab213480) and BD Sciences (568085). Supplementary Table S1 list the other antibodies, reagents, and chemicals.

Mice

C57BL/5 mice (The Jackson Laboratory, Bar Harbor, ME, USA) aged 5 to 6 weeks were purchased. All animal experiments were conducted per the protocol approved by Chungnam National University (approval number: 202003 A-CNU-064) and adhered to the Korean Food and Drug Administration guidelines. Each experimental group consisted of at least five mice, and each experiment was repeated thrice at the minimum.

Cell lines

MRC5 fibroblasts were obtained from the Nagendra Lab at KW (Seoul, Korea). The cells were grown in DMEM containing 10% (v/v) FBS and 1% penicillin/streptomycin (PS, Welgene), respectively. Murine Lewis lung cancer (LLC) (CRL-1642™) and 4T1 (CRL-3406™) cells were purchased from the American Type Culture Collection (ATCC) and cultured in Roswell Park Memorial Institute (RPMI) media (LM001-05, Welgene) containing 10% fetal bovine serum (FBS; Biowest) and 1% PS.

Bone marrow-derived DCs were obtained from C57BL/6 mice using an established method [25]. Isolated cells cultured with RPMI medium (Thermo, USA)

supplemented with 10 U/mL penicillin, 10 µg/mL streptomycin, 2 mM L-glutamine (Gibco, USA), 20 ng/mL murine granulocyte macrophage-colony stimulating factor (GM-CSF), 10 ng/mL IL-4, and 10% FBS at 37 °C and 5% CO_2 to differentiate DCs. The cells were incubated for 6–7 days, and non-adherent cells were collected.

Cell viability assay

Cell viability was measured using a CCK-8 (Cell Counting Kit-8, Dojindo, Kumamoto, Japan) and CellTiter-Glo®Assay (CTG, luminescent cell viability assay, G7572, Promega) according to the manufacturer's instructions, which detect viable cells by quantifying ATP.

LLC or 4T1 cells (1.5×10^4/well of 96-well plates) or DCs (2×10^4/well of 96-well plates) were cultured overnight and treated with PTM at the indicated dilute concentrations for 24 h.

PYR (Invitrogen) was used at 1 mM/mL. N-acetyl-l-cysteine (NAC; Sigma) was added at a 10 mM concentration; cPTIO (2-(4-carboxyphenyl)-4,4,5,5-tetramethylimidazoline-1-oxyl-3-oxide, Cayman) was used at 0.1 mM concentration. CTG reagent (50 µL) and 50 µL of cell medium were incubated and shaken for 10 min under light with an integration time of 3 s. It was subsequently quantified using a microplate reader (Synergy HT, Biotek).

Annexin/propidium iodide (PI) assay

Lewis lung cancer cells (LLCs) (2×10^4/12-well plate) and DCs (5×10^5/24-well plate), stained using Annexin and PI, were analyzed using flow cytometry (Fortessa™, BD Biosciences). DCs were isolated using the APC surface marker, $CD11c^+$, and a flow cytometer (Fortessa, BD Biosciences). Cells were acquired for 10,000 events and gated using FlowJo v10 (Tree Star, Inc.).

ROS production in the mitochondria

The cells were plated on 15-mm coverslips at a density of 6×10^4 cells per 24-well plate and left overnight. For mitochondrial ROS (mROS) production, the cells were exposed to 25% PTM for 5 h and subsequently stained with 3 µM MitoSox™ red and 250 nM MitoTracker™ green (catalog no. CMXRos M7512; Invitrogen) for 30 min at CO_2, 37 °C. Images were obtained using a ZEISS LSM900 confocal microscope (ZEISS Microscopy).

Immunofluorescence

First, 15-mm coverslips were fixed with 3% paraformaldehyde overnight and washed thrice with Dulbecco's phosphate-buffered saline (DPBS). The coverslips were incubated with 0.1% Triton X-100 for 10 min for cell membrane permeabilization. The samples were incubated with 1% bovine serum albumin (BSA) solution in PBS containing 0.1% Tween-20 (PBST) for 1 h to prevent nonspecific antigen binding. After washing thrice, the coverslips were incubated with anti-calreticulin (CRT, 1:1000), anti-high mobility group box 1 (HMGB1, 1:1000) or PD-L1 (1:1000) in 1% BSA/PBST overnight at 4 °C. After washing thrice, the coverslips were incubated with a secondary antibody (1:250) for 1 h. The nuclei were stained with Hoechst 33,342 for 5 min. Subsequently, the coverslips were mounted with a mounting medium (Dako, Glostrup, Denmark) at 4 °C overnight. Confocal images were analyzed using a ZEISS LSM 900 microscope (Carl Zeiss Microscopy). Images were analyzed using a Zen Blue lite 2. We examined at least 20 cells under each condition and determined the means showing statistical significance ($p<0.05$) using GraphPad Prism 8.

PD-L1 expression in vitro in the LLC cells

LLCs were pretreated with PBS (control), 12.5, or 25% PTM for 4 h, then cultured with 10 ng/mL of IFN-γ for 24 h. Next, cells were incubated with INF-γ (10 ng/mL) alone as the positive control.

DCs cultured alone and co-cultured with tumor cells in a transwell system

First, DCs were seeded at a density of 1×10^6 cells/well before PTM treatment. To test DC activation, the upper and lower layers were cultured separately with 1×10^6 (on day 6 of differentiation) per well of DCs and 2×10^5 per well of LLC cells. A Transwell system (37012, SPL) was used. The LLC cells that adhered to the surface were treated with PTM at the indicated concentrations and co-cultured with the DCs. LPS (100 ng/mL) was used as a positive control. After 24 h, the DCs were harvested and stained with $CD11c^+$-APC, MHC II-FITC, CD40-PE, CD80-BV650, and CD86-BV510. Before analysis, each marker was compensated using compensation beads (UltraComp ebeads™, Invitrogen, Life Technologies Corporation Eugen. OR USA). Then, surface markers were analyzed using flow cytometry and acquired for 10,000 events. Data were analyzed using Flow-Jo v.10.

Cytokine measurements

Tumor necrosis alpha (TNF-α), IL (interleukin)-1β, and IL-10 from the supernatants were measured using an enzyme-linked immunosorbent assay (ELISA), following the manufacturer's instructions (Invitrogen). Cytokine secretion was measured in triplicates via four independent experiments.

Immunoblotting

The cells were lysed with the Tris lysis buffer containing 10 mM of Tris-HCl, at pH 7.5, 50 mM of NaF, 1% w/v of NP-40, 100 mM of NaCl, 1% sodium deoxycholate, 0.1% w/v SDS, phosphate inhibitors, and protease inhibitors. Cell lysates (25 mg of protein extracts) were

separated via 10% SDS-polyacrylamide gel electrophoresis and transferred onto nitrocellulose membranes. The blots were incubated with primary antibodies, phospho-STAT1 (1:1000), STAT1(1:1000), PD-L1(1:1000), or CRT (1:1000), overnight at 4 °C, and subsequently washed thrice with TBST (0.1% Tween® 20, tris-buffered saline). The blots were then incubated with secondary goat anti-rabbit IgG H&L (1:10000) for 2 h at room temperature. Imaging and quantification of band intensities were performed using the BioRad imaging system. Images represent at least three independent experiments.

Quantitative real-time PCR (qRT-PCR)

Total RNA was isolated using TRIzol reagent (Invitrogen). RNA concentration and purity, defined as the ratio of absorbance at 260 and 280 nm (A260/A280 nm), were measured using a NanoDrop ND-1000 (Qiagen GmbH, Hilden, Germany). Next, cDNA was synthesized from total RNA using AccuPower Cycle Script RT Premix (dT20, Bioneer, Daejeon, Korea). Real-time two-step PCR was used to amplify the sequences of interest using a 2× Rotor-Gene SYBR Green PCR kit (204076, Qiagen) and the Rotor-Gene 3000 system (Qiagen). Fold induction was determined by comparing it to the control of 18 S rRNA. The primer sequences are shown (Supplementary Table S2).

Mice treatment using PTM and activating DCs with PTM

Wild-type LLCs (5×10^5) were subcutaneously injected with 0.1 mL PBS into the right flank of six-week female C57BL6 mice. Three or four days after LLC cell injection, mice developed palpable tumors, upon which 50% PTM was administered via subcutaneous injection around the tumor at a volume of 200 µL per mouse in Hanks' balanced salt solution (HBSS) without phenol red on days 4, 7, 10, 13, and 16. PTM was filtered through a 0.22 µm Durapore® PVDF Membrane Filter. Simultaneously, DC (3×10^5/200 µL) was also intraperitoneally injected into the flank (i) without stimulation (unstim.DCs) or (ii) with 6.3% PTM stimulation (stim.DCs) for 24 h. Tumor sizes are calculated as Length × Width^2/2. The tissues for fluorescence-activated cell sorting (FACS) were isolated and analyzed 9 d after cell injection. Tumor tissues were cut into 2–4 mm fragments before digestion via a Miltenyi Tumor Dissociation Kit (Miltenyl Biotec, 130-096-730) with an optimized protocol. Spleen tissues were sliced into small pieces and physiologically homogenized. After digestion, the tissues were passed through a Falcon 70-µm cell strainer to produce single-cell suspensions. RBCs were lysed in RBC lysis buffer. Single cells were stained using a Live-Dead Fixable Violet Dead Cell Kit (Invitrogen) at room temperature for 20 min, washed with PBS, and stained with lymphocyte antibodies for 30 min in the dark. Data acquisition encompassed 100,000 events using a Fortessa™ flow cytometer, while subsequent data analysis and gating were performed using Flow-Jo v.10.

Isolation of DCs from tumor tissues

First, we prepared single-cell suspension tumor isolation from the mouse using a tumor cell isolation kit (Miltenyl Biotec, 130-096-730). Tissues were minced and digested enzyme mix by adding 2.35 ml of RPMI 1640, 100 µL of Enzyme D, 50 µL of Enzyme R, and 12.5 µL of Enzyme A into a gentleMACS C tube. The cells or tumor-infiltrating DC cells were then purified immunomagnetically by two to three rounds of positive selection with CD11c (N418) MicroBeads (Miltenyi Biotec, 130-125-835) according to the manufacturer's instructions. FACS analyzed the purity of DCs, which was 88% in wild-type spleen.

Tumor cell isolation

Before isolating the tumor, we prepared the wash buffer and the tumor dissociation kit. Single cells from the tumor tissues were resuspended in 5 mL of TryPLE (Gibco, 12604013) express enzyme and 2 µL of DNase I (Roche, final concentration 4 U/mL). The cells were then incubated in a shaker at 37 °C for 10 min. After two washes, the cells spun down at 450 x g for 5 min at 20–30 °C. The cell suspension was filtered through a 70 µM cell strainer and a 40 µM cell strainer. The cell pellet was immediately resuspended in RBC lysis buffer, followed by the addition of a cell culture medium.

Statistical analyses

Graph Pad Prism 8 was used to perform statistical analyses. The data are expressed as the mean ± standard error of the mean (SEM). The means of two independent groups were compared using an unpaired Student's *t*-test. In contrast, those of multiple groups were compared using either a one-way or a two-way analysis of variance (ANOVA) test. Survival curves were plotted using the log-rank (Mantel–Cox) test.

Results

Generation of reactive H2O2 and NO2 molecules in medium

The optical emission spectrum (OES) acquired various plasma species NO, OH, and reactive-N_2 excited by a non-thermal plasma jet (NTPJ) (Fig. 1b). The N_2^* metastatic state predominantly interacts with water, leading to hydroxyl radicals being generated via the dissociation of water molecules [24, 26]. OH and H molecules, produced after N_2^* disappears, initiate subsequent reactions at the water surface. In the plasma jet, N atoms tend to disappear via the $N+O_2\rightarrow NO+O$ reaction, as dictated by their reaction coefficient [27]. The DMEM was treated with NTPJ without PYR for 5 min, and H_2O_2

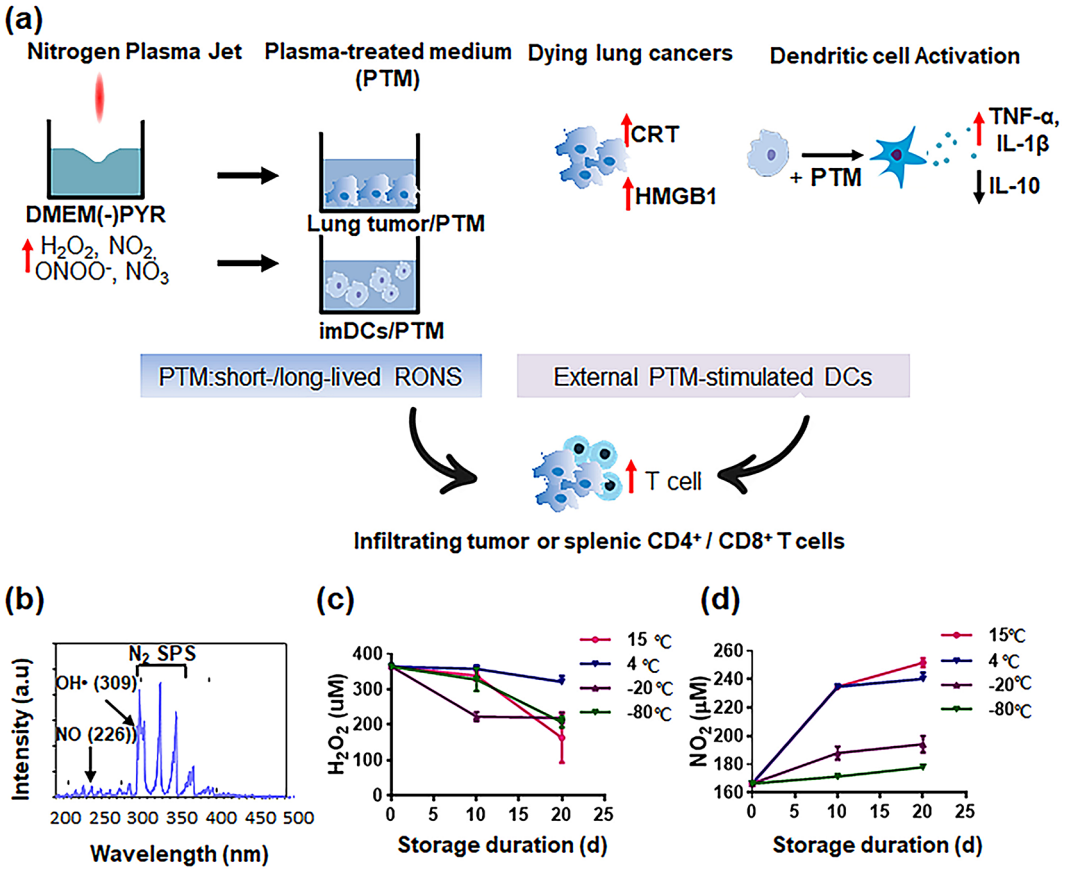

Fig. 1 PTM-stimulated DCs combined with PTM enhance antigen-specific T cells in cancer immune responses. (**a**) A scheme to increase the number of tumor-infiltrating lymphocytes involves the activation of extracellular DCs while concurrently introducing plasma-treated medium (PTM) treatment to inhibit tumor progression and activate immune T cells. (**b**) Optical emission spectrum (OES) of a non-thermal plasma jet with nitrogen at 200–500 nm. (**c-d**) H_2O_2 and NO_2 concentrations corresponding to PTM stored at 15 ℃, 4 ℃, −20 ℃, and −80 ℃ for 10 or 20 d, determined using Amplex™ Red Reagent and Griess reagent assay, respectively. Results presented as the mean ± SEM of three replicates. These experiments were analyzed using a two-tailed unpaired Student's *t*-test. **p* < 0.01 (15 ℃), 20 d vs. PTM immediately following the preparation (0 d); ***p* < *0.01* (4 ℃ or 20 ℃), 10 or 20 d vs. 0 d. ***p* < *0.01* (−80 ℃), 20 d vs. 0 d

and NO_2 remained stable according to storage conditions (Fig. 1c-d). The H_2O_2 concentration (350±45 μM) in PTM remained unchanged for 10 d at 4 °C, 15 °C, and −80℃ under all conditions (Fig. 1c). Nitrite (NO_2) concentrations at 15 °C and 4 ℃ were substantially increased by day 10 and remained steady after that; however they did not change considerably under storage conditions of −20℃ or −80℃ (Fig. 1d). These results suggested that PTM could be stored for 10 d at 15 °C until needed for the subsequent bioactivity assay after generation.

PTM induces selective toxicity in tumor cells only

PTM-treated cells exhibit cytotoxic responses [11, 28]. To confirm the cytotoxic effect exerted by PTM on lung cells, we conducted a series of assays to examine the effects exerted by PTM on the viability of MRC5 normal lung cells, tumors cells (LLC and 4T1 cells), and primary cells (DCs). The effect of each treatment after 24 h treatment is shown relative to that of the control. Although 50% PTM exerted minor cytotoxic effects on MRC5 lung normal cells, neither of the other PTM dilutions exhibited any toxicity (Fig. 2a). PTM treatment induced cell death in tumor cells (LLC and 4T1 cells) as well as in primary cells (DCs) in a dose-dependent manner. Although 12.5% PTM treatment did not induce cell death in any of the cells tested, 25% PTM induced cell death in tumor cells; there is toxicity observed in DCs compared with that in the untreated control (**p*<0.05) (Fig. 2b-d). By contrast, higher PTM concentrations (50%) induced substantial cell death in LLC cells (80.21±10.52%) and 4T1 cells (65.56±8.20%) as well as in DCs (45.23±5.21%), although cell death in DCs was at a significantly lower level than that induced in LLC cells.

We utilized ATP luminescence-based viability tests to determine whether PTM induces cell death in LLC cells and DCs pretreated with antioxidants, such as PYR, NAC, and cPTIO. We confirmed that PTM-induced cell death was higher in LLC cells than in DCs and that

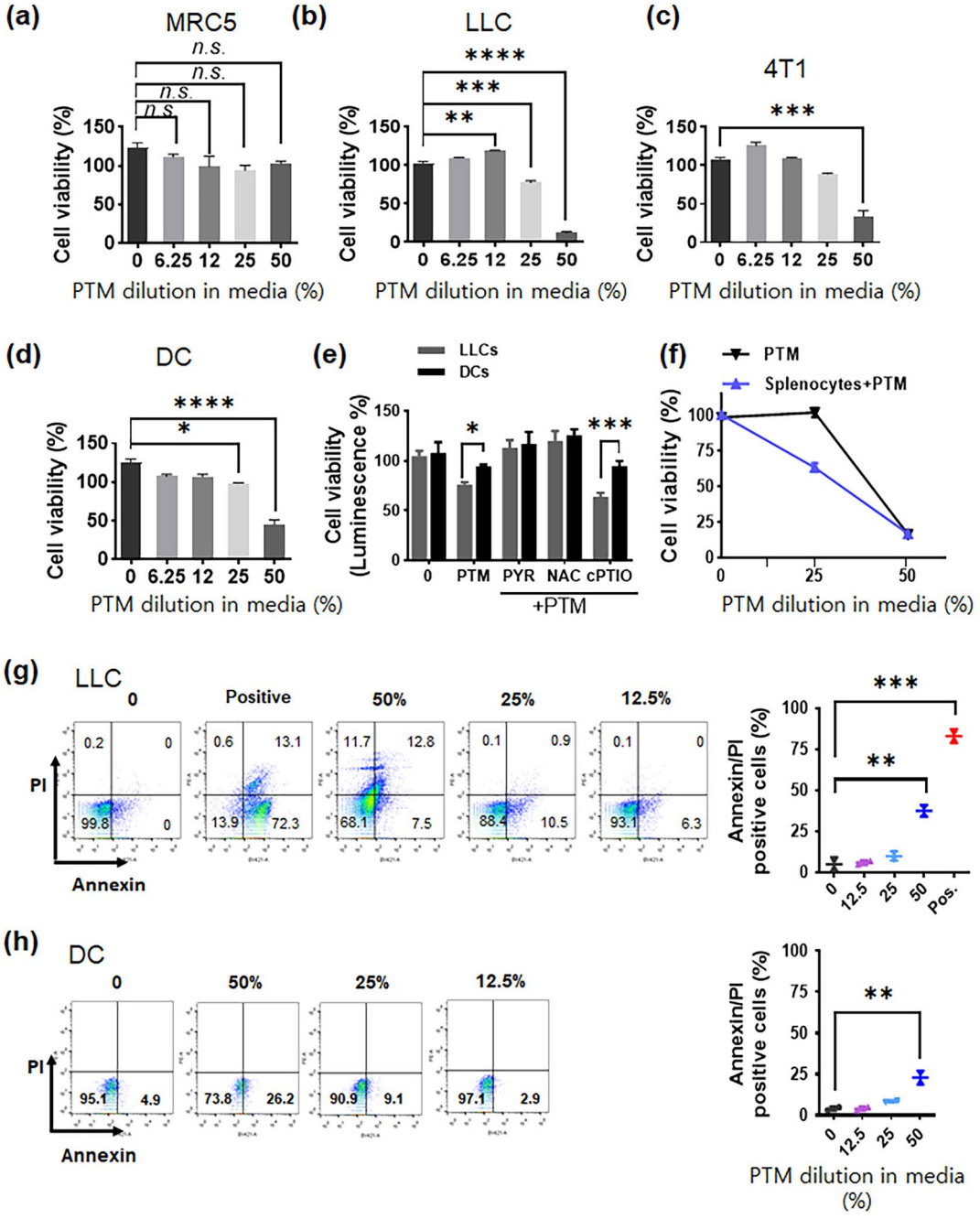

Fig. 2 Plasma-treated medium (PTM) induces a cytotoxic effect and alterations in LLC cells. (**a**) Lung normal MRC5 cells, (**b-c**) tumor cells (LLC or 4T1 cells), and (**d**) primary cells (DC) were incubated with various concentrations of PTM (6.25, 12.5, 25, and 50%) for 24 h. Cell viability was determined using CCK-8 assays. This experiment was repeated thrice. Statistical significance was analyzed via one-way ANOVA; $^{*}p < 0.05$, $^{**}p < 0.01$, $^{***}p < 0.001$, and $^{****}p < 0.0001$ compared to the control. *n.s.*, not significant. (**e**) On day 1, intracellular ATP in LLC or DCs were assayed using luciferase-based viability following treatment with 25% PTM alone or pre-incubation with 2 mM PYR, 10 mM NAC, and 0.1 mM cPTIO for 1 h before PTM treatment. The mean ± SEM represents data; $^{*}p < 0.05$ and $^{***}p < 0.001$; two-way analysis of variance (ANOVA). (**f**) LLCs were incubated alone (25% or 50% PTM) or co-cultured with splenocytes (1×10^5/well of 96-well plates) in the presence of PTM. Cell viability was assessed using CCK-8 assays. (**g-h**) LLC and DC cell death incubated in various PTM was evaluated via Annexin/PI staining and flow cytometry, respectively. The positive sample inactivates heated at 100℃ for 10 min. Results are represented by the means ± SD from three independent experiments. Significant differences were determined via a two-way ANOVA; $^{**}p < 0.01$ and $^{***}p < 0.001$ compared to the control

this was abolished by pre-incubation with PYR or NAC; however, not with cPTIO (Fig. 2e). Next, we utilized splenocytes and evaluated LLC cell viability following co-culturing. As shown in Fig. 2f, splenocytes enhanced LLC cell death under 25% PTM treatment. Flow cytometry analysis indicated that 25% PTM slightly decreased the viability of LLC cells and DCs compared with that of the control (Fig. 2g-h). In comparison, 50% PTM substantially reduced the viability of both cell types.

PTM treatment enhances ROS generation and oxidative stress-mediated signaling in tumor and normal cells

ROS, such as superoxide anion, hydrogen peroxide, and hydroxyl radical, can cause injury to cells. The total superoxide generation of LLC cells was determined using an immunofluorescent probe. LLC cells exposed to 25% PTM for 6 h exhibited higher MitoSOX red fluorescence (mROS, mitochondrial superoxide probe) than the control (Fig. 3a). The PTM-induced red fluorescence intensity was significantly reduced by pretreatment with the ROS scavenger, NAC; however, not with the NO scavenger, cPTIO.

A qRT-PCR analysis was conducted to assess the genes' expression in oxidative stress in tumor cells and normal lung MRC5 cells. Total RNA from PTM-exposed cells was extracted after 5 h of incubation because intracellular ROS was much higher than immediately. Figure 3b shows the transcriptional response to PTM, indicating the involvement of genes related to detoxifying hydrogen peroxides, such as Gpx1 and CAT enzymes. These enzymes protect against hydrogen peroxide [29, 30]. The increase in ataxia-telangiectasia mutated serine/threonine kinase (ATM) levels in tumor cells is associated with DNA repair and recombination [31].

In Gpx1 gene, the expression levels of 50% or 25% PTM-exposed tumor cells were significantly enhanced by 2.8-fold and 2.5-fold, respectively (Fig. 3b and Supplementary Fig. S3b). Moreover, CAT levels were enhanced to 50% (~2.2-fold) or 25% (~1.8-fold) with PTM treatment (Fig. 3c and Supplementary Fig. S3c). As shown in Figs. 3d and 50% PTM significantly increased ATM levels in tumor cells. In contrast, PTM treatment did not increase the expression of Gpx1, CAT, and ATM in the normal lung cells. Higher ROS generation in PTM in tumor cells elevated oxidative stress levels, leading to the detoxification of ROS [32].

PTM enhances CRT exposure on the cell surface and HMGB1 secretion in the cytoplasm

Elevated ROS levels within the TME substantially enhanced ICD and tumor-infiltrating lymphocyte (TIL) function [33, 34]. Therefore, we performed Immunofluorescence staining to analyze CRT exposure and HMGB1 localization in PTM-treated cells with or without ROS or NO scavengers. Compared with untreated cells, PTM treatment induced a considerable amount of CRT translocation to the cell membrane, which was abolished by NAC pretreatment yet not by cPTIO (Fig. 4a). Similarly, HMGBI translocation into the cytoplasm was markedly enhanced by PTM treatment. Furthermore, pre-incubation with NAC inhibited PTM-mediated HMGB1 translocation, yet this was not observed with cPTIO (Fig. 4b). Nuclear HMGB1 co-localization was considerably decreased in the cells exposed to PTM alone as in those pretreated with cPTIO. PTM altered CRT and HMGB1 localization by elevating intracellular ROS and H_2O_2.

PTM inhibits IFN-γ-upregulated PD-L1 expression

We investigated whether PTM affected the IFN-γ-mediated PD-L1 expression in LLC cells. Western blot data indicated that IFN-γ substantially enhanced PD-L1 expression in LLC cells. In contrast, PTM pretreatment markedly attenuated the PD-L1 expression induced by IFN-γ (Fig. 5a and Supplementary Figure S4a). Confocal and FACS analyses consistently indicated that IFN-γ-induced PD-L1 expression was considerably inhibited by PTM (Fig. 5b and c). STAT1 is a well-known signal molecule downstream of the IFN-γ receptor [35]. Therefore, we investigated whether PTM dampens this process by attenuating STAT1 phosphorylation (pSTAT1). PTM inhibited STAT1 phosphorylation induced by IFN-γ (Fig. 5d and Supplementary Fig.S4b). The results indicate that PTM antagonizes IFN-γ induced PD-L1 expression in LLC cells.

PTM induces DC activation

Tumor-associated DCs in the immunosuppressive TME are mainly responsible for inhibiting antitumor immune responses. Additionally, DCs are essential in activating T cells to regulate the TME [36]. We prepared immature bone marrow-derived cells, up to 77.5% of which could be derived from mouse bone marrow cells following stimulation with GM-CSF (Supplementary Fig. S5a). Next, we analyzed the expression of surface molecules in DCs treated with different PTM concentrations. PTM treatment increased the expression levels of CD80/86, MHC I and II, and CD40 in DCs in a dose-dependent manner (Fig. 6a-c and Supplementary Fig. S5b). Inverted phase-contrast microscopy, which was used to examine DC morphology, indicated that the size and acquired cytoplasmic projections (dendrites) in 6.25% of PTM-stimulated DCs were higher than those of unstimulated DCs (Supplementary Fig. S5c). DCs exhibit stellate processes that create a veiled appearance, which aligns with their typical morphological characteristics [37].

Tumor cells modulate the functions of immune cells, such as DCs or macrophages, thereby creating a tumor-friendly environment. Therefore, we investigated whether

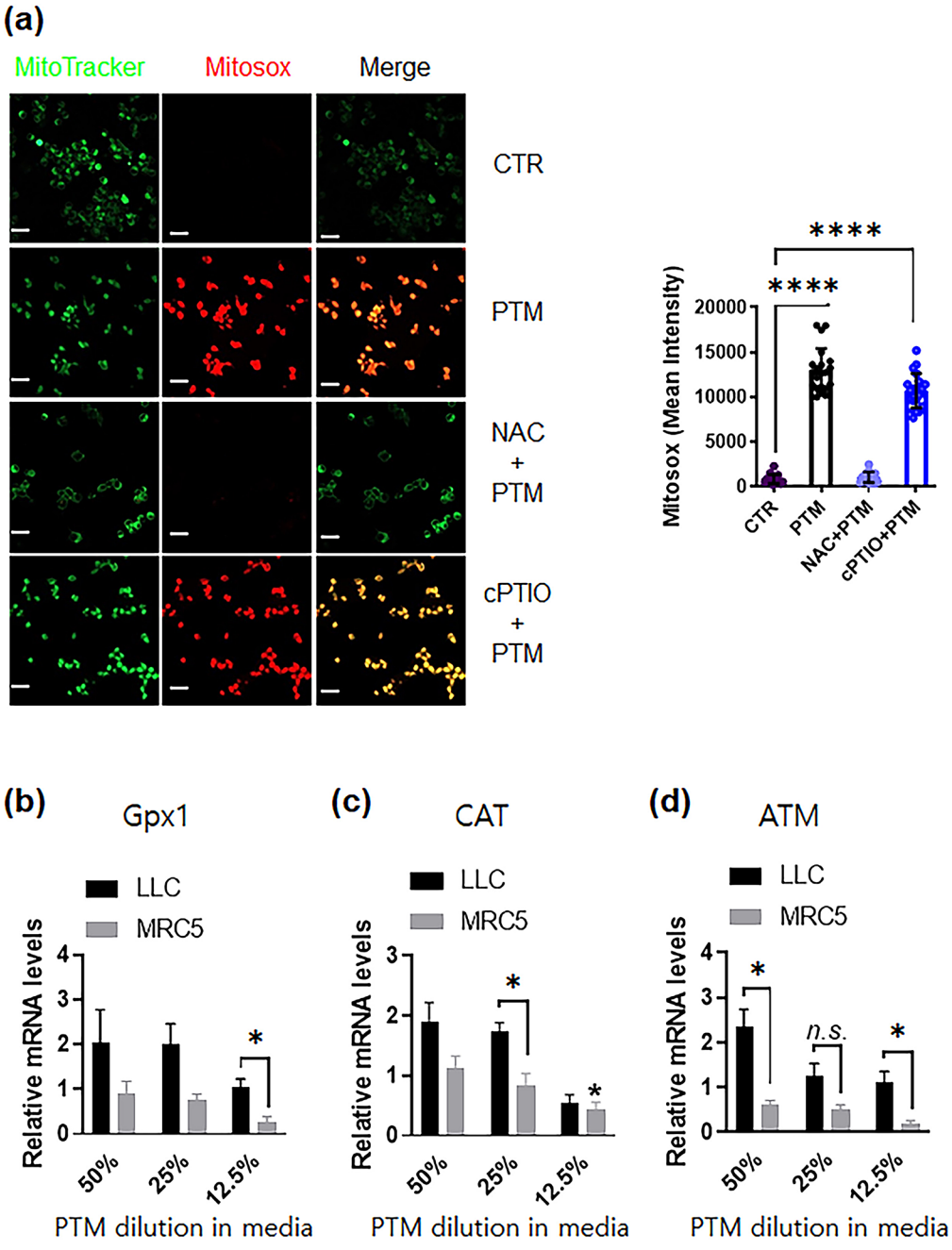

Fig. 3 Plasma-treated medium detoxifies antioxidant enzymes in LLC or MRC5 cells. (**a**) (Left) Representative confocal microscopy images indicate MitoTracker (green) and Mitosox (red) staining of LLCs incubated in different conditions: the control, 25% PTM, and 25% PTM pre-incubated with 10 mM NAC or 0.1 mM cPTIO for 5 h; scale bar, 10 μM. (Right) The intensity of red fluorescence was quantified using Zen blue software; $n = 20$, 25, 19, and 27 single cells for control, PTM alone, and PTM incubation with pre-incubated NAC or cPTIO, respectively. The mean ± SED represents results from three independent experiments. Unpaired Student's *t*-test was used to calculate statistical significance; ****$p < 0.0001$. (**b-d)** PTM stimulates anticancer signals in LLCs or normal lung MRC5 cells. The mRNA expression of Gpx1 (glutathione peroxidase), CAT (catalase), and ATM gene was quantified by qRT-PCR. Fold changes of the three target genes were normalized using the 18 S mRNA or GAPDH control. $n = 3$, mean ± sem. *$p < 0.05$, *n.s.*, not significant

tumor cells affect DC activation. LLC cells were co-cultured with DCs using a transwell with a pore size of 0.4 μM and then exposed to different PTM concentrations (Supplementary Fig. S5d). CD80 molecule expression induced by PTM in DCs was markedly suppressed when co-cultured with LLC cells (Fig. 6a). No differences were observed between CD40 and MHC class II expression levels with or without tumor cells (Fig. 6b-c). The cytokines produced by PTM-treated cells were determined using ELISA (Fig. 6d-f). No substantial TNF-α, IL-1β,

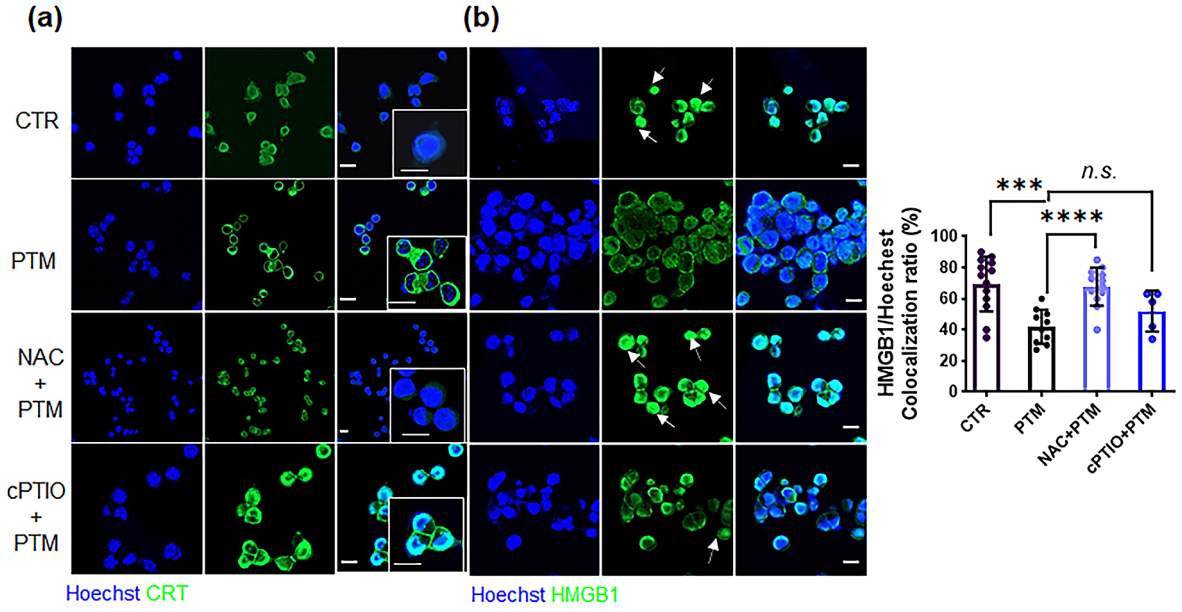

Fig. 4 PTM increases CRT exposure and cytoplasmic translocation of HMGB1 from the nucleus of LLCs. (**a**) Surface-exposed CRT (green) and (**b**) translocated HMGB1 (green) in LLCs treated with medium (CTR), 25% PTM, pretreated 10 mM NAC, or 0.1 mM 2-(4-carboxyphenyl)-4,4,5,5-tetramethylimidazoline-1-oxyl-3-oxide(cPTIO) and subsequently with 25% PTM for 12 h. Confocal images indicate stained nuclei (blue), and CRT or HMGB1 (green); scale bar, 10 μm. Arrows indicate increased fluorescence intensity of HMGB1 in the nuclei. Quantitative co-localization of HMGB1 expressed as nuclear (Hoechst) (n) per cell. HMGB1 staining intensity was analyzed using Zen blue lite. Data are represented by the mean ± standard error of the difference between two means (SED) and calculated using a two-tailed unpaired Student's *t*-test. This experiment was repeated thrice; ***$p < 0.001$, and ****$p < 0.0001$ *n.s.*, not significant

and IL-10 production was observed in the PTM-treated LLC cells compared to those in untreated LLC cells. PTM treatment to stimulates higher TNF-α production in the supernatants (Fig. 6d) in DCs and LLC cells co-culture condtions, which leads to increased DC maturation. We hypothesized that this effect is directly related to DC activation in the TME. Compared with untreated DCs, PTM-treated DCs produced considerable levels of IL-1β and IL-12, which were markedly suppressed by co-culturing LLC cells (Fig. 6e and Supplementary Fig. S5e). IL-10 production in unstimulated DCs was undetectable but dramatically increased by LLC co-culturing. Furthermore, PTM stimulated DCs to produce IL-10, markedly suppressed by LLC co-culturing (Fig. 6f).

PTM-activated DCs enhance antitumor activity of PTM

We hypothesized that PTM and DCs may display synergistic antitumor activity based on the above results. Thus, LLCs (5×10^5) were subcutaneously injected into the right flank of C57BL/6 mice. After tumorigenesis was confirmed by palpation approximately 3 d or 4d after injection, the mice were randomly grouped and injected with PBS or PTM with or without unstimulated DCs or PTM (6.3%)-stimulated DCs (Fig. 7a). Mice were subcutaneously injected at the base area or the intratumoral region of the tumor with 200 μL of 50% PTM and concurrently injected intraperitoneally with PTM-stimulated DCs or unstimulated DCs at indicated times. No specific differences in body weight were observed between the groups (Supplementary Fig. S6a). Tumor growth in PTM-injected mice was inhibited compared with that in the PBS-injected control group; however, the difference was insignificant (Fig. 7b-c and Supplementary Fig. S6b). The antitumor effect of PTM was markedly enhanced by DC injection. Tumor volume was the lowest in the group injected with PTM/PTM-stimulated DCs (Fig. 7b-c and Supplementary Fig. S6b).

Next, the T cell composition of the spleen and TILs were analyzed via FACS (Supplementary Fig. S7d-e). The $CD4^+$ T cell number in the splenocytes of the groups injected with PTM/PTM-stimulated DCs was markedly higher than that in the PTM-alone, control groups or PTM/unstim.DCs. The $CD8^+$ T cell number in the groups injected with PTM/PTM-stimulated DCs was also significantly higher than that in the control group or other groups (Supplemenatary Fig. S7d). The $CD8^+$ TIL number was highest in the group injected with PTM/PTM-stimulated DCs compared to the other groups. The number of $CD4^+$ TILs was significantly higher in groups injected with PTM/unstim.DCs or PTM/PTM-stimulated DCs than in the control or PTM-alone group and was considerably higher in the groups injected with PTM/PTM-stimulated DCs than in the PTM/unstim. DCs (Supplementary Fig. S7e). Finally, we determined each group's 40 d mouse survival rate (Fig. 7d). The group injected with PTM/PTM-stimulated DCs exhibited

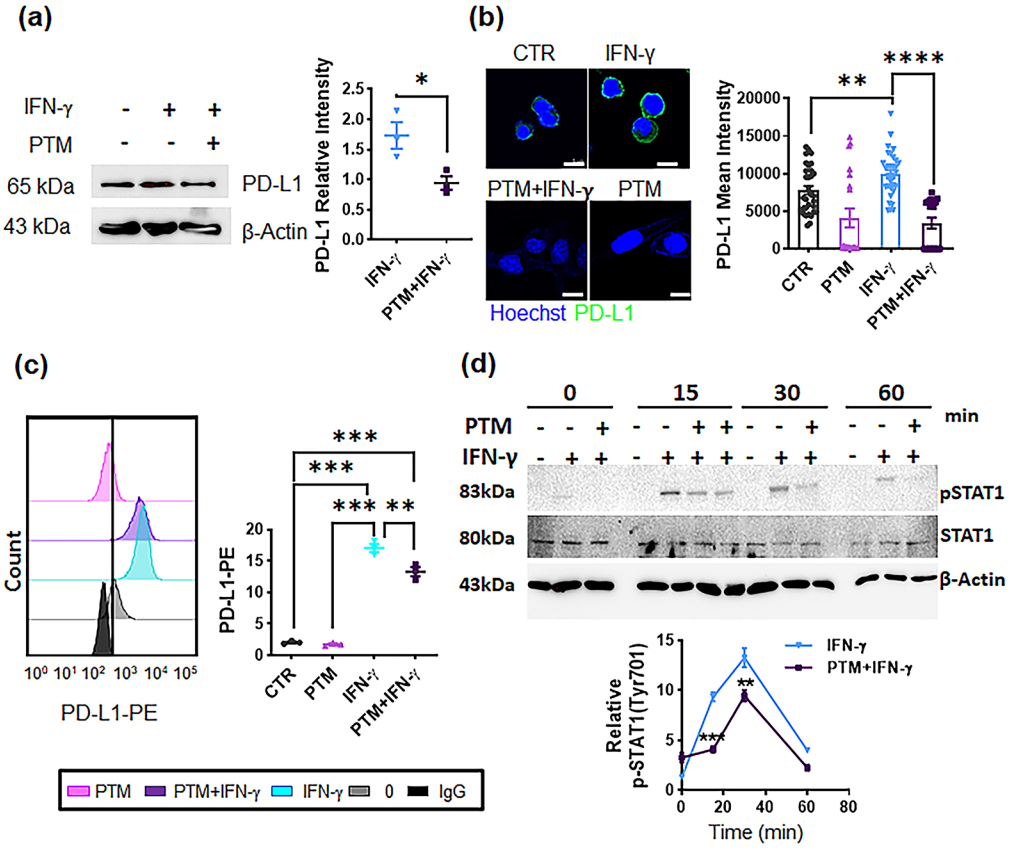

Fig. 5 PTM inhibits IFN-γ-induced PD-L1 expression and attenuates STAT1 phosphorylation in LLCs. (**a-c**) LLCs were incubated with medium, and pre-treated-PTM (12.5%) for 4 h and subsequently treated with IFN-**γ** (10 ng/mL) for 24 h. A positive sample was used for IFN-γ treatment (10 ng/mL). (**a**) PD-L1 expression was detected via western blot. The PD-L1 (relative to β-actin) expression was calculated using Image J. Statistical significances were estimated using a two-way analysis of variance (ANOVA); mean ± SEM; $n = 3$, $^{*}p < 0.05$. (**b**) Confocal images indicate stained nuclei (blue) and mouse PD-L1 (green) being merged; scale bar, 10 μM. Mean fluorescence intensities were subsequently quantified using Zen blue; $n = 20$, 18, 20, and 18 single cells were used for control, PTM alone, IFN-γ, and PTM/IFN-γ, respectively; $^{**}p < 0.01$, and $^{****}p < 0.0001$. *n.s.*, not significant. (**c**) Flow cytometric analysis of PD-L1-PE was observed using Flowzo ($n = 3$). The graph indicates PD-L1 levels (clone 9A11) normalized by the IgG control. Statistical significance was determined via one-way ANOVA. Data are represented by the mean ± SEM of four representative experiments: $^{**}p < 0.01$, and $^{***}p < 0.001$. (**d**) PTM markedly reduced IFN-γ-induced STAT1 phosphorylation at the indicated times. Cells were incubated with IFN-γ alone (positive control), and 12.5% PTM for 4 h, and subsequently treated with IFN-γ (10 ng/mL) at the indicated times; "–", before indicated times (0, 15, 30, 60 min) indicates negative control. STAT1 phosphorylation (pSTAT1) at Tyr701, as well as at total STAT1 (relative to β-actin), was detected using western blot analysis. Line charts illustrate quantification data about pSTAT1 levels at indicated time points compared to levels induced by IFN-γ stimulation from the positive control group. Statistical differences between IFN-γ and IFN-γ/PTM were determined via a two-way ANOVA. Data are represented by the mean ± SEM of three independent experiments: $^{***}p < 0.001$ (15 min) and $^{**}p < 0.01$ (30 min)

significantly better survival than the untreated control group ($p = 0.0453$). On day 40, one mouse was in the PTM-injected group, and two in the PTM/unstim. DC-injected group and four in the PTM/PTM-stimulated DC-injected group survived.

Discussion

This study demonstrated that PTM- or PTM-stimulated DCs, or a combination of both, exhibited a considerable antitumor effect in a mouse skin model. The impact of ROS on biological systems varies depending on their concentration [38, 39]. Lower hydrogen peroxide concentrations regulate cytokines in DCs and growth factors [40]. Elevated ROS accumulation is pivotal in providing a survival advantage during cancer progression, a phenomenon that is further heightened during chemotherapy [38]. Tanaka et al. have recently reported a novel technique of irradiating culture medium with non-equilibrium atmospheric pressure plasma (NEAPP) to obtain plasma-activated medium (PAM). The culture of glioblastoma cells and normal astrocyte cells in cells in PAM resulted in selective apoptotic death of the glioblastoma cells [41]. Cancer cells have higher ROS levels than normal cells due to increased metabolism [42]. As a result, cancer cells are more likely to cross the critical ROS threshold when exogenous ROS stress is applied [43]. This leads to both lethal damage and apoptosis. This model has been used to explain the basic strategy behind

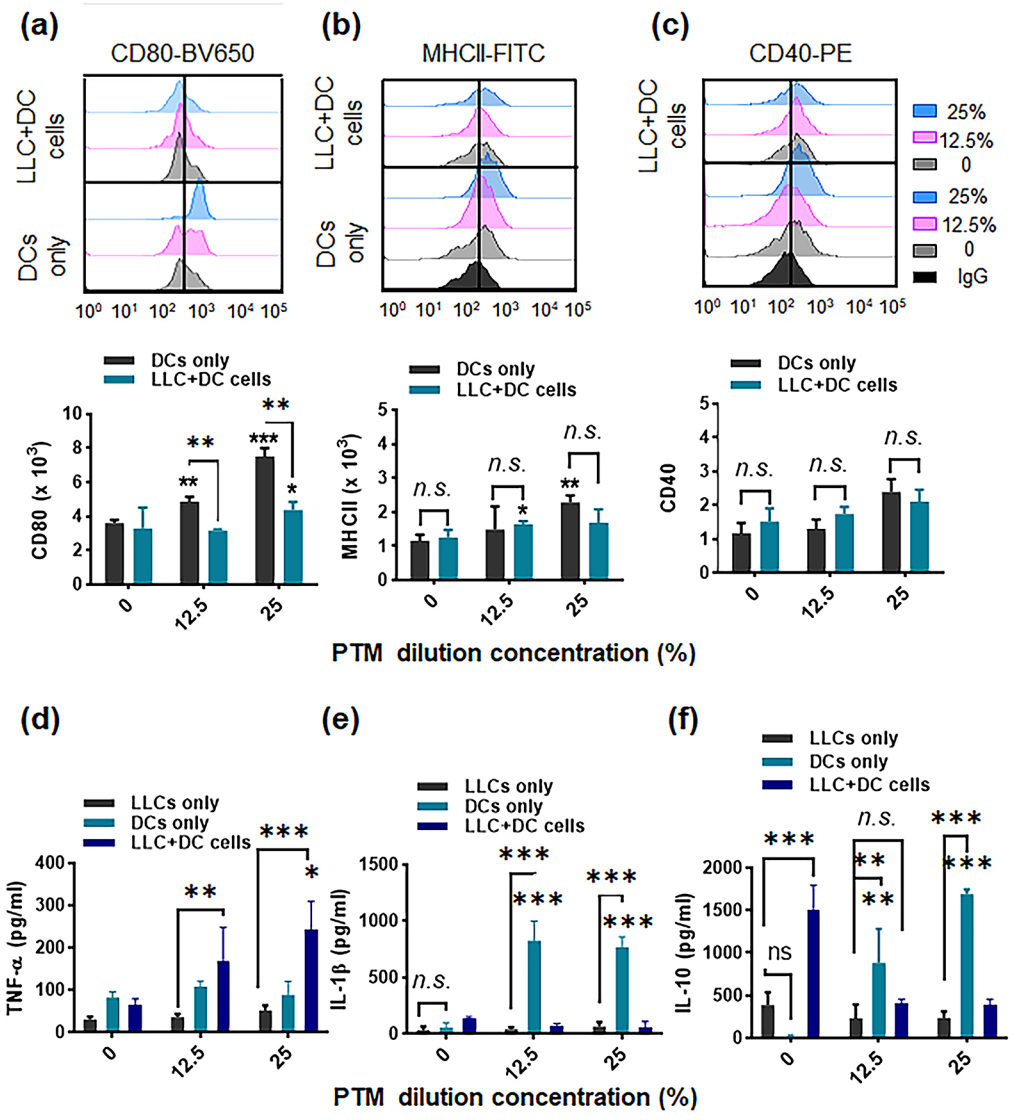

Fig. 6 Plasma-treated medium (PTM) stimulates dendritic cells (DCs) alone and in a co-culture system. DCs were incubated alone (12.5 or 25% PTM) or co-cultured with Lewis lung cancer (LLC) cells in the presence of PTM. The DCs were cultured either alone or separated by a transwell system. After 24 h, surface marker expression was determined. (**a-c**). Representative histograms and bar plots demonstrate CD80-BV650, MHCII-FITC, and CD40-PE levels in the DCs only or in DCs with the co-culture, using flow cytometry, respectively. The data were analyzed and gated using FlowJo. The statistical significance of the difference between DC-alone and tumor cell co-culture groups was determined via a two-way ANOVA; $*p<0.05$ and $**p<0.01$; n.s., insignificant. Concurrently, data compared to the untreated cells using a two-tailed unpaired Student's *t*-test are shown; $*p<0.05$ and $**p<0.01$, mean ± SEM; $n=4–5$. (**d-f**) The TNF-α, IL-1β, and IL-10 levels in the supernatants from LLC cells, DCs cultured alone, DCs incubated with tumor cells, and both treated with 12.5% or 25% PTM, were measured. Comparison between LLCs, DCs, and LLC + DC cells using a two-way ANOVA; $**p<0.01$, and $***p<0.001$. *n.s.*, not significant. Statistical significance was determined using a two-tailed unpaired Student's *t*-test; $*p<0.05$, $**p<0.01$, and $***p<0.001$; $n=4$

developing drugs that exploit the significant differences in ROS-mediated metabolism. Tumor cells proliferate rapidly and are often under high oxidative stress, making them more sensitive to internal and external stimuli. One potential anticancer strategy is to exacerbate the oxidative stress by increasing the levels of ROS, which further aggravates the oxidative stress within the cancer cells. In our study, we observed a significant increase in the levels of ROS in cancer cells treated with PTM compared to normal cells (Fig. 3 and Supplementary Fig.S3). This difference in ROS behavior between cancer and normal cells helps explain the disparity in cell mortality and survival rates. As noted, high concentrations of 50% Plasma-activated medium (PAM) resulted in dendritic cell (DC) toxicity, highlighting that DCs are more fragile compared to normal lung cells when exposed to plasma treatments. Our findings suggest that the moderate to high concentrations of reactive species in PAM can significantly influence the metabolic functions of DCs, including mitochondrial and lysosomal activities, which

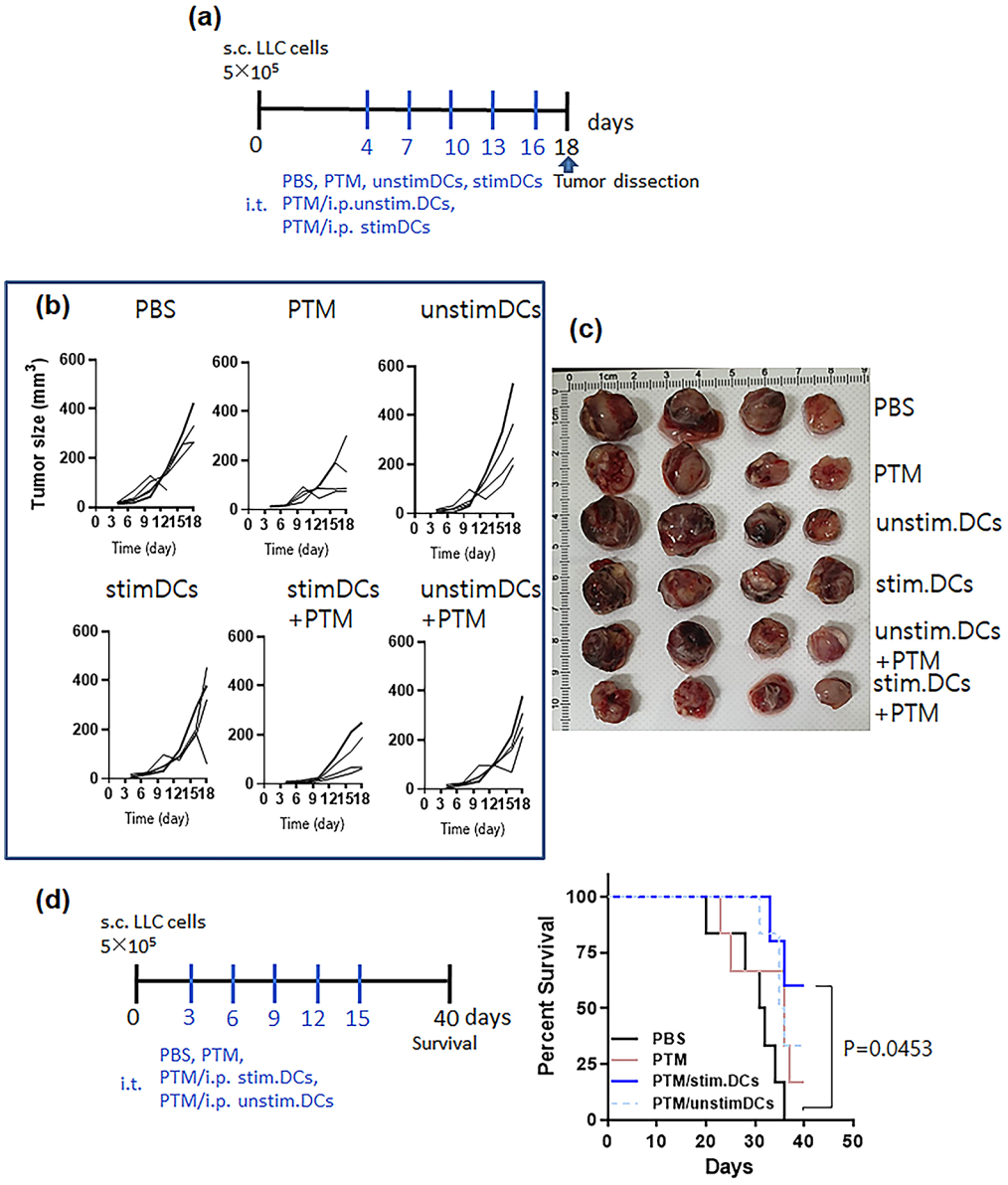

Fig. 7 PTM combined with PTM-stimulated DCs decreases tumor size and increases immune responses. (**a**) The treatment schedule for a mouse tumor model injected with Lewis lung cancer (LLC) cells ($n=4$ per group). Unstimulated DCs or 6.25% stimulated DCs were injected intraperitoneally at 3-d intervals after LLC tumor formation. (**b**) Tumor growth curves. Each line indicates tumor growth in an individual mouse. $n=2$. (**c**) On day 18, photographs of isolated tumors in the six groups were taken. (**d**) Mouse survival throughout the predetermined study period of 40 d was assessed, and the survival curves were plotted using the Log-rank with Mantel-Cox test (6 mice per group); $^{*}p=0.0453$. $n=2$

are more pronounced than in normal cells. Therefore, we have adopted a strategy of direct administration to the tumor, which preserves the DCs while directly targeting and killing the tumor. We found that 12.5% of PTM did not exert cytotoxic effects on tumor cells and DCs. Furthermore, PTM activated DCs at its lowest concentration (6.25%) and induced ICD at 25% (Fig. 4). Tumor-associated antigens (TAAs) that were released from dying cells in situ are presented, indicating that even 12.5% PTM had reduced IFN-γ- induced PD-L1 expression (Fig. 5).

IFN-γ, a type II interferon, is crucial for innate and adaptive immunity. Various cell types, including T cells, macrophages, and natural killer (NK) cells, secrete IFN-γ [44]. IFN-γ is an essential cytokine in the TME, strongly inducing PD-L1 expression in cancer cells and possibly contributing to tumor immune evasion [45, 46]. The results indicate that IFN-γ signaling is transmitted from the IFN-γ receptor to its downstream JAK-STAT1 pathway, following which activated JAK1 and JAK2 phosphorylate STAT1 on tyrosine 701, causing phosphorylated STAT1 to homodimerize [35, 47].

Subsequently, dimerized STAT1 translocates into the nucleus and binds to the GAS (IFN-γ-activated sites) elements to initiate a series of IFN-γ-regulated gene transcriptions, including that of PD-L1. PD-1/PD-L1 pathway blockade-based immunotherapy is a paradigm-shifting therapeutic approach that has been proven effective in treating several cancer types, receiving multiple FDA approvals for clinical application [48–50]. Interestingly, we observed that PTM inhibited PD-L1 expression following IFN-γ stimulation in vitro. H_2O_2/ROS in the PTM induce cancer ICD, release TAAs from dying cells in situ, and secrete pro-inflammatory cytokines and co-stimulatory molecule expression by mature DCs in vitro. Therefore, we used externally stimulated DCs and PTM in mouse tumor-suppressive experiments. We observed that the effect of PTM on cell viability depended on cell density [11, 23]. Therefore, we used higher PTM concentrations to confirm tumor growth. However, a limitation of our study is the apparent lack of a considerable antitumor effect in the PTM-alone group, possibly due to the small sample size.

Although no considerable tumor size reduction between unstimulated DCs and PTM-stimulated DCs was observed, reducing the infusion number may have revealed a meaningful difference. DCs, which are well known to generate ROS and nitric oxide, also produce antimicrobial peptides, enabling them to mount a direct attack against recognized pathogens. High LPS concentrations (5–10 ug/mL) have been reported when cytotoxic activity is induced in human immature peripheral blood monocyte-derived DCs [51]. Notably, even at a low dose (10 ng/mL), LPS triggered apoptosis in human killer dendritic cells (hkDCs). Using autologous cytotoxic DCs has opened up crucial new prospects in cancer immunotherapy. Notably, these hkDCs killed cancer as well as normal cells. Herein, we used the lowest PTM concentration (6.3%), which is not even used for DC activation at the cellular level. We hypothesized that the ROS/H_2O_2 generated by PTM contributes to DC activation and enables them to migrate to lymph nodes. Our results demonstrated that PTM treatment alone stimulates DCs, leading to higher secretion of pro-inflammatory cytokines (IL-12, IL-1β) and the suppression of anti-inflammatory IL-10 secretion.

The safety of PTMs is a crucial factor in determining their clinical application. PTM was observed to inhibit LLC cell survival sans H_2O_2 degradation when stored at 4 ℃, 15 ℃, and 80 ℃ for a minimum of ten d, but not at −20 ℃. Previous reports have demonstrated that H_2O_2 is more unstable when stored at −30 °C in a freezer than at 4 °C [11]. Nitrite concentration in PTM markedly increased over time when stored at 4 °C and 15 °C, whereas only a minimal change was observed when stored at −20 °C and −80 °C. This suggests that the nitrite concentration in PTM does not contribute to its cytotoxic effects. Therefore, PTM should be stored at −80 °C–15 °C when intended for use within 10 d. The findings of this study may be applied to designing current DC-based vaccines [52, 53] and indirect pathways that induce robust cytotoxic T lymphocyte responses and DC-dependent tumor cell toxicity. Our study demonstrated, for the first time, that antitumor immune responses were induced by replacing activated immunosuppressive/tolerant DCs, which have lost their ability to present antigens around the tumor, with DC activation at concentrations that do not affect DC toxicity. The concentration refers to the optimal level that promotes DC activation without causing harm to the DCs. These stimulated DCs can be frozen for extended storage periods and used again to treat patients with cancer and other diseases. Our future goal is to study the time-dependent effects of low temperatures on PTM-stimulated DC aging, their anticancer functions, and cellular metabolism in the TME. Furthermore, this study highlights the potential of PTM as an alternative therapeutic approach to reactivating host immunity in the TME, particularly when combined with externally activated DC therapy or an immune checkpoint inhibitor.

In summary, H_2O_2 is crucial for eliciting ICD danger signals, including CRT and HMGB1, among the ROS produced by PTM. PTM specifically reduced LLC cell levels of IFN-γ-induced pSTAT1 Y701, leading to downregulated PD-L1 expression. Additionally, PTM can enhance DC function in conjunction with PTM-stimulated DCs, significantly boosting immune responses and cytotoxic $CD8^+$ T cell infiltration. Such a possibility would result in slower tumor growth and longer survival times.

Lastly, we utilized splenocytes and evaluated LLC cell viability following co-culturing (Supplementary Fig.S12c). The graph shows splenocytes enhanced LLC cell death under 50% or 25% PTM treatment. In future studies, it will be necessary to further investigate the mechanisms by which splenocytes or lymph nodes and their separation, such as macrophages, DCs and T cells, enhance LLC cell death under PTM treatment.

Abbreviations

PTM	Plasma-treated medium
NTPJ	Non-thermal plasma jet
DCs	Dendritic cells
NSCLC	Non-small cell lung cancer
ROS	Reactive oxygen species
RNS	Reactive nitrogen species
H_2O_2	Hydrogen peroxide
NO_2	NO_3,Nitrite oxides
ICD	Immunogenic cell death
PYR	Sodium pyruvate
Gpx1	Glutathione peroxidase
CAT	Catalase
ATM	Ataxia Telangiectasia Mutated
cPTIO	2-(4-carboxyphenyl)-4,4,5,5-tetramethylimidazoline-1-oxyl-3-oxide

NAC	N-acetyl-l-cysteine
LLC	Lewis lung cancer
CRT	Calreticulin
HMGB1	High mobility group box 1
IL	Interleukin
STAT1	Signal transducer and activator of transcription 1
PD-L1	Programmed death-ligand 1
IFN-γ	Interferon-gamma
TNF-α	Tumor necrosis alpha
TILs	Tumor-infiltrating lymphocytes

Supplementary Information

The online version contains supplementary material available at https://doi.org/10.1186/s12935-024-03569-x.

Supplementary Material 1

Supplementary Material 2

Supplementary Material 3

Supplementary Material 4

Acknowledgements
We thank SK Gurmessa (Oregon Health and Science University) for providing excellent technical assistance.

Author contributions
CBL. and HJK. prepared the concept of this manuscript and acquired the primary funding. CBL. NK. and HJK. wrote the main manuscript text and discussed methodology. SKG was first taught in vivo tumor formation. CBL. made plasma jet source. HGC. prepared Fig. 3. CBL. ITJ. and ZJ. prepared Figs. 6 and 7. HJK. is the supervisor. All authors reviewed the results and commented on the manuscript.

Funding
The Basic Science Research Program supported this research through the National Research Foundation of Korea (NRF), funded by the Ministry of Education (RS-2023-00247685) and ICT and Future Planning (2020R1A2C1008826).

Data availability
No datasets were generated or analysed during the current study.

Declarations

Ethics approval and consent to participate
The Institutional Research and Ethics Committee of Chungnam National University approved all animal experiments (approval number: 202003 A-CNU-064), which complied with the relevant guidelines of the Korean Food and Drug Administration.

Competing interests
The authors declare no competing interests.

Author details
[1]Department of Microbiology, College of Medicine, Chungnam National University, Daejeon 35015, Korea
[2]Department of Internal Medicine, College of Medicine, Chungnam National University, Daejeon 35015, Korea
[3]Department of Molecular Microbiology and Immunology, Oregon Health and Science University, 3181 SW Sam Jackson Park Rd, Portland, OR 97239, USA
[4]Department of Medical Devices, National Institute of Pharmaceutical Education and Research Guwahati (NIPER-G), Kamrup, Assam 781101, India
[5]Department of Electrical and Biological Physics, Plasma Bioscience Research Center, Kwangwoon University, Seoul 01897, Korea
[6]Department of Medical Sciences, Chungnam National University, Daejeon 35015, Korea

Received: 27 July 2024 / Accepted: 9 November 2024
Published online: 23 November 2024

References

1. Wu F, Fan J, He Y, Xiong A, Yu J, Li Y, et al. Single-cell profiling of tumor heterogeneity and the microenvironment in advanced non-small cell lung cancer. Nat Commun. 2021;12:2540.
2. Chen Z, Fillmore CM, Hammerman PS, Kim CF, Wong K-K. Non-small-cell lung cancers: a heterogeneous set of diseases. Nat Rev Cancer. 2014;14:535–46.
3. Domagala-Kulawik J. The role of the immune system in non-small cell lung carcinoma and potential for therapeutic intervention. Translational lung cancer Res. 2015;4(2):177.
4. Katopodi T, Petanidis S, Charalampidis C, Chatziprodromidou I, Eskitzis P, Tsavlis D, et al. Tumor-infiltrating dendritic cells: decisive roles in cancer immunosurveillance, immunoediting, and tumor T cell tolerance. Cells. 2022;11:3183.
5. Gardner A, Ruffell B. Dendritic cells and cancer immunity. Trends Immunol. 2016;37(12):855–65.
6. Zong J, Keskinov AA, Shurin GV, Shurin MR. Tumor-derived factors modulating dendritic cell function. Cancer Immunol Immunother. 2016;65:821–33.
7. Gardner A, Ruffell B. Dendritic cells and cancer immunity. Trends Immunol. 2016;37:855–65.
8. Yan D, Sherman JH, Keidar M. Cold atmospheric plasma, a novel promising anticancer treatment modality. Oncotarget. 2017;8:15977.
9. Heirman P, Van Boxem W, Bogaerts A. Reactivity and stability of plasma-generated oxygen and nitrogen species in buffered water solution: a computational study. Phys Chem Chem Phys. 2019;21:12881–94.
10. Khalili M, Daniels L, Lin A, Krebs FC, Snook AE, Bekeschus S, et al. Non-thermal plasma-induced immunogenic cell death in cancer. J Phys D. 2019;52:423001.
11. Adachi T, Tanaka H, Nonomura S, Hara H, Kondo S, Hori M. Plasma-activated medium induces A549 cell injury via a spiral apoptotic cascade involving the mitochondrial-nuclear network. Free Radic Biol Med. 2015;79:28–44.
12. Poramapijitwat P, Thana P, Sukum P, Liangdeng Y, Kuensaen C, Boonyawan D. Selective cytotoxicity of lung cancer cells—A549 and H1299—Induced by ringer's lactate solution activated by a non-thermal air plasma jet device, Nightingale®. Plasma Chem Plasma Process. 2023;43(4):805–30.
13. Bekeschus S, Scherwietes L, Freund E, Liedtke KR, Hackbarth C, von Woedtke T, et al. Plasma-treated medium tunes the inflammatory profile in murine bone marrow-derived macrophages. Clin Plasma Med. 2018;11:1–9.
14. Chen C, Zhou S, Yang X, Ren M, Qi Y, Mao Y, et al. In vitro study of cold atmospheric plasma-activated liquids inhibits malignant melanoma by affecting macrophage polarization through the ROS/JAK2/STAT1 pathway. Biomed Pharmacother. 2024;175:116657.
15. Azzariti A, Iacobazzi RM, Di Fonte R, Porcelli L, Gristina R, Favia P, et al. Plasma-activated medium triggers cell death and the presentation of immune activating danger signals in melanoma and pancreatic cancer cells. Sci Rep. 2019;9(1):4099.
16. Yan L, Sundaram S, Rust BM, Picklo MJ, Bukowski MR. Metabolomes of Lewis lung carcinoma metastases and normal lung tissue from mice fed different diets. J Nutr Biochem. 2022;107:109051.
17. Cheng Y-J, Lin C-K, Chen C-Y, Chien P-C, Chuan H-H, Ho C-C, et al. Plasma-activated medium as adjuvant therapy for lung cancer with malignant pleural effusion. Sci Rep. 2020;10(1):18154.
18. Freund E, Liedtke KR, van der Linde J, Metelmann H-R, Heidecke C-D, Partecke L-I, et al. Physical plasma-treated saline promotes an immunogenic phenotype in CT26 colon cancer cells in vitro and in vivo. Sci Rep. 2019;9:634.
19. Galluzzi L, Buqué A, Kepp O, Zitvogel L, Kroemer G. Immunogenic cell death in cancer and infectious disease. Nat Rev Immunol. 2017;17(2):97–111.
20. Garg A, Dudek-Peric AM, Romano E, Agostinis P. Immunogenic cell death. Int J Dev Biol. 2015;59(1):131–40.
21. Fang T, Cao X, Shen B, Chen Z, Chen G. Injectable cold atmospheric plasma-activated immunotherapeutic hydrogel for enhanced cancer treatment. Biomaterials. 2023;300:122189.
22. Svensson-Arvelund J, Cuadrado-Castano S, Pantsulaia G, Kim K, Aleynick M, Hammerich L, et al. Expanding cross-presenting dendritic cells enhances oncolytic virotherapy and is critical for long-term antitumor immunity. Nat Commun. 2022;13(1):7149.
23. Lee CB, Lee KI, Kim YJ, Jang IT, Gurmessa SK, Choi EH, et al. Non-thermal plasma jet-treated medium induces selective cytotoxicity against Mycobacterium tuberculosis-infected macrophages. Biomedicines. 2022;10(6):1243.

24. Lee CB, Na YH, Hong T-E, Choi EH, Uhm HS, Baik KY, et al. Evidence of radicals created by plasma in bacteria in water. Appl Phys Lett. 2014;105(7):073702.
25. Sauter M, Sauter RJ, Nording H, Olbrich M, Emschermann F, Langer HF. Protocol to isolate and analyze mouse bone marrow derived dendritic cells (BMDC). STAR Protocols. 2022;3(3):101664.
26. Uhm HS, Ki SH, Baik KY, Choi EH. Influence of oxygen on generation of reactive chemicals from nitrogen plasma jet. Sci Rep. 2018;8(1):9318.
27. Baulch D, Bowman CT, Cobos CJ, Cox RA, Just T, Kerr J, et al. Evaluated kinetic data for combustion modeling: supplement II. J Phys Chem Ref Data. 2005;34:757–1397.
28. Lin A, Truong B, Patel S, Kaushik N, Choi EH, Fridman G, et al. Nanosecond-pulsed DBD plasma-generated reactive oxygen species trigger immunogenic cell death in A549 lung carcinoma cells through intracellular oxidative stress. Int J Mol Sci. 2017;18:966.
29. Orian L, Cozza G, Maiorino M, Toppo S, Ursini F. *Glutathione*. CRC Press; 2018:53 – 7.
30. Zhao Y, Wang H, Zhou J, Shao Q. Glutathione peroxidase GPX1 and its dichotomous roles in cancer. Cancers. 2022;14:2560.
31. Guleria A, Chandna S. ATM kinase: much more than a DNA damage responsive protein. DNA Repair. 2016;39:1–20.
32. Privat-Maldonado A, Schmidt A, Lin A, Weltmann K-D, Wende K, Bogaerts A et al. ROS from physical plasmas: Redox chemistry for biomedical therapy. Oxid Med Cell Longev. 2019;2019.
33. Malla R, Surepalli N, Farran B, Malhotra SV, Nagaraju GP. Reactive oxygen species (ROS): critical roles in breast tumor microenvironment. Crit Rev Oncol/Hematol. 2021;160:103285.
34. Kuo C-L, Chou H-Y, Chiu Y-C, Cheng AN, Fan C-C, Chang Y-N, et al. Mitochondrial oxidative stress by Lon-PYCR1 maintains an immunosuppressive tumor microenvironment that promotes cancer progression and metastasis. Cancer Lett. 2020;474:138–50.
35. Platanias LC. Mechanisms of type-I-and type-II-interferon-mediated signalling. Nat Rev Immunol. 2005;5(5):375–86.
36. Banchereau J, Steinman RM. Dendritic cells and the control of immunity. Nature. 1998;392(6673):245–52.
37. Tan Y-F, Leong C-F, Cheong S-K. Observation of dendritic cell morphology under light, phase-contrast or confocal laser scanning microscopy. Malays J Pathol. 2010;32:97–102.
38. Yang H, Villani RM, Wang H, Simpson MJ, Roberts MS, Tang M, et al. The role of cellular reactive oxygen species in cancer chemotherapy. J Exp Clin Cancer Res. 2018;37:1–10.
39. Chio IIC, Tuveson DA. ROS in cancer: the burning question. Trends Mol Med. 2017;23:411–29.
40. Pazmandi K, Magyarics Z, Boldogh I, Csillag A, Rajnavolgyi E, Bacsi A. Modulatory effects of low-dose hydrogen peroxide on the function of human plasmacytoid dendritic cells. Free Radic Biol Med. 2012;52:635–45.
41. Tanaka H, Mizuno M, Ishikawa K, Nakamura K, Kajiyama H, Kano H, et al. Plasma-activated medium selectively kills glioblastoma brain tumor cells by down-regulating a survival signaling molecule, AKT kinase. Plasma Med. 2011;1:3–4.
42. Nakamura H, Takada K. Reactive oxygen species in cancer: current findings and future directions. Cancer Sci. 2021;112(10):3945–52.
43. Yan D, Talbot A, Nourmohammadi N, Sherman JH, Cheng X, Keidar M. Toward understanding the selective anticancer capacity of cold atmospheric plasma—A model based on aquaporins. Biointerphases 2015;10(4).
44. Schoenborn JR, Wilson CB. Regulation of interferon-γ during innate and adaptive immune responses. Adv Immunol. 2007;96:41–101.
45. Mandai M, Hamanishi J, Abiko K, Matsumura N, Baba T, Konishi I. Dual faces of IFNγ in cancer progression: a role of PD-L1 induction in the determination of pro-and antitumor immunity. Clin Cancer Res. 2016;22:2329–34.
46. Kharma B, Baba T, Matsumura N, Kang HS, Hamanishi J, Murakami R, et al. STAT1 drives tumor progression in serous papillary endometrial cancer. Cancer Res. 2014;74:6519–30.
47. Schmitt MJ, Philippidou D, Reinsbach SE, Margue C, Wienecke-Baldacchino A, Nashan D, et al. Interferon-γ-induced activation of Signal Transducer and activator of transcription 1 (STAT1) up-regulates the tumor suppressing microRNA-29 family in melanoma cells. Cell Communication Signal. 2012;10(1):1–14.
48. Gong J, Chehrazi-Raffle A, Reddi S, Salgia R. Development of PD-1 and PD-L1 inhibitors as a form of cancer immunotherapy: a comprehensive review of registration trials and future considerations. JITC. 2018;6:1–18.
49. Sun C, Mezzadra R, Schumacher TN. Regulation and function of the PD-L1 checkpoint. Immunity. 2018;48:434–52.
50. Xu L, Zhang Y, Tian K, Chen X, Zhang R, Mu X, et al. Apigenin suppresses PD-L1 expression in melanoma and host dendritic cells to elicit synergistic therapeutic effects. J Exp Clin Cancer Res. 2018;37:1–15.
51. Lakomy D, Janikashvili N, Fraszczak J, Trad M, Audia S, Samson M, et al. Cytotoxic dendritic cells generated from cancer patients. J Immunol. 2011;187:2775–82.
52. Santos PM, Butterfield LH. Dendritic cell–based cancer vaccines. J Immunol. 2018;200:443–9.
53. Zhou F, Ciric B, Zhang G, Rostami A. Immunotherapy using lipopolysaccharide-stimulated bone marrow-derived dendritic cells to treat experimental autoimmune encephalomyelitis. Clin Exp Immunol. 2014;178(3):447–58.

Publisher's note